HHS Public Access

Author manuscript

Adv Opt Mater. Author manuscript; available in PMC 2022 January 18.

Published in final edited form as:

Adv Opt Mater. 2021 January 18; 9(2): . doi:10.1002/adom.202001217.

Hydrogel-based diffractive optical elements (hDOEs) using rapid digital photopatterning

Zheng Xiong[1,2], **Puskal Kunwar**[1,2], **Pranav Soman**[1,2,*]

[1.]Department of Biomedical and Chemical Engineering, Syracuse University, Syracuse, NY, USA, 13244

[2.]Syracuse Biomaterials Institute, Syracuse, NY, USA, 13244

Abstract

Hydrogels, due to their optical transparency and biocompatibility, have emerged as an excellent alternative to conventional optical materials for biomedical applications. Advances in microfabrication techniques have helped convert conventional hydrogels into optically functional materials such as hydrogel-based diffraction optical elements (hDOEs). However, key challenges related to device customization and ease/speed of fabrication need to be addressed to enable widespread utility and acceptance of hDOEs in the field. Here, we report rapid printing of customized hDOEs on polyethylene glycol diacrylate (PEGDA) hydrogel using digital photopatterning; a novel method that combines simulated computer-generated hologram (SCGH) and projection photolithography. To showcase the versatility of this approach, a range of hDOEs are demonstrated, including 1D/2D diffraction gratings, Dammann grating, Fresnel zone plate (FZP) lens, fork-shaped grating and computer-generated hologram (CGH) of arbitrary pattern. Results demonstrate that printed hDOEs exhibit optical performance that is comparable with devices made with conventional materials. This versatile strategy can be potentially implemented with other photosensitive hydrogels to achieve user-defined hDOEs in a time-efficient and cost-effective fashion.

Graphical Abstract

* psoman@syr.edu.

Conflict of interest

The authors declare no conflict of interest.

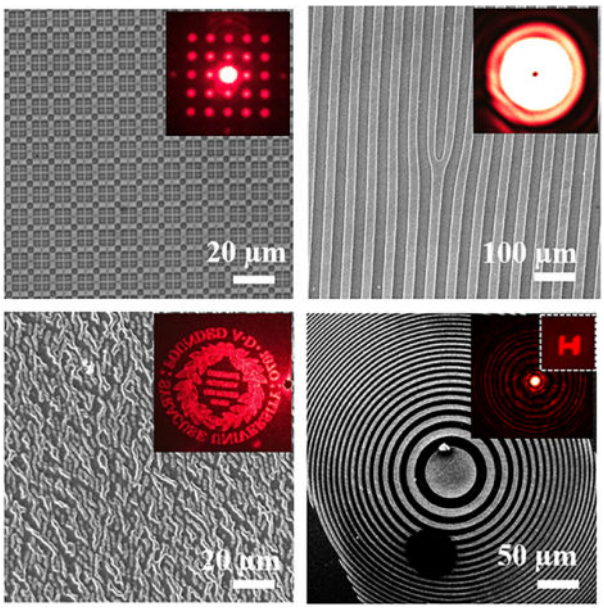

Keywords

hydrogel; diffractive optics; photopatterning; customization; projection printing

1. Introduction

Hydrogels, which recapitulate biophysical and biochemical properties of extracellular matrix, have made significant impact in many biomedical fields, such as, drug delivery, regenerative medicine, tissue engineering, bio-sensing, flexible electronics and microfluidics.[1–6]Continued advances in polymer chemistry have demonstrated that functional properties can be introduced within hydrogels to transform them into ‘smart’ materials. This has led to the development of hydrogels with customizable properties such as the abilities to change shapes, resist mechanical forces, release target enzymes and exhibit electrical, magnetic as well as optical properties.[7–14]

Inspired by natural systems, microstructural modification has been exploited as a promising strategy to introduce new optical properties to conventional materials such as manipulation of light based on diffraction or diffraction optical elements (DOEs).[15–18]These DOEs have become increasingly important in biomedical applications ranging from imaging to diagnostics to sensing.[19–22] In the past decades, the DOEs are mostly made of conventional optical materials such as glass, semiconductor, and metals. Nonetheless, the inherent lack of mechanical flexibility and biocompatibility of these materials render their use difficult for *in vitro* and *in vivo* biophotonics applications. Hydrogels, due to their unique optical transparency and biocompatibility, provides a good alternative to conventional optical materials. Several natural and synthetic hydrogels, such as, silk, chitin, chitosan, bovine serum albumin, polyacrylamide, polyacrylic acid and PEGDA have been used to make hydrogel based DOEs or hDOEs with optical performance comparable to conventional materials.[22–28]However, competing challenges such as high resolution, ease/cost of

manufacturing, and customization of design based on target applications, prevent its widespread use in the field.

At present, hDOEs such as diffraction grating, holographic components, and Fresnel zone plates (FZP) are fabricated using indirect and direct methods.[7,22,26,29–31] Indirect methods, such as mask-based photolithography, inverse opals, soft lithography, and nanoimprinting, require use of expensive physical masks, and time-consuming iterative optimization to fabricate hDOEs. On the other hand, direct methods such as electron beam lithography, direct laser writing, and multi-beam interference lithography do not require physical mask to fabricate high-resolution hDOEs, however challenges with scalability and long processing/fabrication times remain. The aforementioned challenges have to be addressed to meet the high demand for hDOEs in the field; this would require an ability to rapidly design and manufacture customized hDOEs based on the needs of target applications.

In this work, we report the design and printing of customized DOEs on synthetic PEGDA hydrogel using digital photopatterning technology which combines digital projection photolithography[32–39] with computer-generated holography[40–42]. In this work, simulated computer-generated holography (SCGH) was used to generate customized digital patterns based on DOE designs, and these digital patterns were uploaded onto a Digital Micromirror Device (DMD) to generate virtual masks (instead of conventional physical masks) to enable rapid printing of hDOEs. To highlight the broad applicability of this method, a range of diffractive devices such as 1D/2D diffraction gratings, Dammann grating, FZP lens, fork-shaped grating and computer-generated hologram (CGH) of arbitrary pattern were designed, printed and their optical performance were compared to DOEs made using conventional materials. To our knowledge, this is the first report introducing SCGH and DMD based digital projection photolithography to print customized hDOEs. This versatile easy-to-implement fabrication strategy can be potentially extended to print hDOEs using other photosensitive hydrogels.

2. Results

2.1 Optical and mechanical characterization of PEGDA

Any material used for making DOEs should exhibit high optical transparency, a refractive index (RI) higher than the background, as well as robust mechanical properties. To meet these requirements, we investigated different concentrations of PEGDA mixed in phosphate buffered saline (PBS) (10, 30, 50, 70 and 90%, v/v). Transmission spectroscopy showed a strong dependency of concentration of PEGDA on its optical transparency (Figure 3A). PEGDA hydrogels above 50% (v/v) had an optical transmission efficiency over 80% in the visible range (400–700 nm). At the concentration below 30%, PEGDA hydrogels pipetted in standard cuvette showed white color possibly due to strong scattering loss in the visible spectrum (Inset in Figure 3A). This results from the polymerization induced phase separation of polymer and solvent, as reported by other groups as well.[43,44]

The refractive index (RI) of PEGDA increased linearly with the prepolymer concentration reaching a maximum of 1.48 and 1.46 for 90% crosslinking and uncrosslinked PEGDA respectively (Figure 3B). The increase in RI has been reported in the literature as a result of

photo-polymerization [44]. As compared to conventional phase-type diffractive optics made in silica/glass where the background RI is typically air, uncrosslinked PEGDA (RI=1.46) is close to RI range of mammalian tissue (~1.35–1.45);[45] this may be beneficial for *in vivo* biophotonic applications. Results show that a ΔRI of 0.0145 will require a thickness of 20 μm to achieve the necessary π phase shift [46] and diffraction/optical performance; use of simple PDMS spacer made this possible.

The elastic modulus increased with higher concentrations of prepolymer solution. (Figure 3C) Low PEGDA concentration samples require constant hydration and often crack during handling. Since 90% PEGDA possessed maximum transparency and ΔRI, and was found to be mechanically robust and easy to handle, this composition was chosen for this study.

2.2 Diffraction grating

Diffraction grating is a diffractive optical device with a periodic structure that splits incident light into several beams in different directions based on the spacing of the periodic structure and the wavelength of the light. Conventional amplitude type phase grating, that consists of an array of transparent and opaque grooves, has lower diffraction efficiency due to loss of light blocked by opaque grooves.[47] As a result, phase-type transmission grating, that consists of π phase transparent grooves, are widely used in the field as they exhibit higher diffraction efficiency. In this work, we designed 1D and 2D phase type transmission gratings based on the relationship between dispersion angle and groove spacing. The property of dispersion when light is normally incident on the micro-optics structures is given by:

$$d\sin\theta_n = n\lambda \tag{1}$$

where d is the groove spacing, n is the diffraction order, λ is the wavelength of the incident light, and θ_n is the diffraction angle of n^{th} diffraction order from the normal,

The digital masks of the gratings were generated as described in section 5. 1D grating was simulated using interference holography between two plane waves while 2D grating utilized crossed addition of two 1D gratings. The theoretical models of 1D and 2D grating are presented in SI-3 (A). The spacing of the interference fringe pattern (d), similar to the groove spacing input, is determined by the angle α between the two plane waves as given below

$$d = \frac{\lambda}{2\sin\left(\frac{\alpha}{2}\right)} \tag{2}$$

In this work, the grooves were designed either to be parallel (1D grating) or perpendicular (2D grating). The inputs for groove spacing is 20 μm while the wavelength of incident light is 632.8 nm. Based on the Equation 2, we calculated the desired angle 1.813° and used it as the initial parameter for the MATLAB algorithm to generate digital masks (Figure 2). The designed patterns of 1D and 2D gratings served as digital masks for the DMD during photo-patterning of PEGDA (Figure 4A). Printed samples were characterized using optical microscopy (Figure 4B), phase contrast microscopy (Figure 4C), and SEM (Figure 4D). For

both 1D and 2D grating, the photo-patterning was able to replicate the 20 μm spacing. SEM images for 2D grating however show some deformation of the pattern possible due to artifacts of sample preparation.

To test the optical performance (angular dispersion) of PEGDA gratings, samples were placed on a slide holder. A monochromatic laser source (632.8 nm) was used to irradiate the samples at a normal angle of incidence, and transmitted diffraction patterns modulated by the gratings were captured on a screen located 100 mm away from the sample and recorded by a digital camera (Figure S1). Figure 4E show the diffraction patterns and their diffraction orders. 1D grating consists of symmetrical spots located on the opposite sides of the screen (X axis), while the diffraction of 2D grating split multiple spots on the horizontal and vertical planes (X and Y axes).

2.3 Dammann grating (Beam Splitter)

Beam splitters are binary-phase Fourier holograms able to convert a single incident beam into an array of identical beamlets at its Fourier plane. Although several methods have been implemented to construct such a device, the most popular one is still the binary diffraction gratings proposed by Dammann. This grating, also known as Dammann Grating (DG), splits the incoming beam into several diffraction orders. At the Fourier plane, these diffraction orders are focused into an array of spots with the same intensity.[47]

Similar with the 2D diffraction grating design described in Sec. 2.2, 2D DG was constructed by using two crossed 1D DG with 5×5 beam splitting. The digital masks were developed via SCGH which simulates Fourier holography of the beam array with DG and array beams having identical intensity distribution. To design DG masks, iterative Fourier transformation was used with the end condition that is Intensity uniformity, U<1% Please refer to Equation 4 and section SI-3 for details. The optimized digital mask is shown in Figure 5A.

Printed PEGDA samples were characterized using microscopy and SEM. The phase contrast between crosslinked pattern of DG (white) and surrounding uncrosslinked prepolymer (black) can be seen in Figure 5C. As mentioned earlier, SEM images show slight deformation of the pattern due to artifacts during sample preparation. The optical performance of DG patterns in PEGDA samples was evaluated as described in Section 2.2 (Figure 5E). Results show that the input laser beam is split into 5 ×5 unique intensity spots. Since the scattering light from central 0^{th} diffraction order affects the intensity profile, we chose the left first column spots and bottom row spots for characterizing the intensity profile along X and Y direction shown in Figure 5F. The intensity uniformity U (Equation 5) along X direction and Y direction are 0.05 and 0.13. These experimental results match well with the theoretical uniformity (U) of 0.01. The slight mismatch could be from scattering at the 0^{th} central diffraction order. PEGDA DG devices can be potentially used for parallel imaging and/or stimulation applications in biophotonics.

2.4 Fresnel zone plate

Fresnel zone plate (FZP) is a flat/planar lens that consists of a series of radially symmetric rings which diffract light to interfere within a focal length at the center to realize an image. Conventional amplitude type FZP, which consists of alternate transparent and opaque zones,

diffracts light from the transparent zones, while phase type FZP, also known as Kinoform phase-type lens, replaces the opaque zones with phase shifting transparent zones.[46] This results in a higher diffraction efficiency for phase type FZP as compared to amplitude type FZP; as a result, phase type FZP has been widely used in integrated optics and biomedicine.

In this work, we designed a phase type FZP with binary microstructure. The mask pattern of FZP displayed on the DMD is designed using SCGH which simulates the interference between spherical wave and plane wave. (refer to SI-3C for details). The radius of successive zones were determined by the distance (f) between dot light source and the holographic plane according to Equation S12. In fact, (f) is also the focal length of FZP according to Equation 6 in section 5. Radius were calculated using the equation $r^2 = fN\lambda$, where r is radius of successive zones, N varying from 1 to 10, λ is the wavelength of light taken as 632.8nm, f is the expected primary focal length as 15.82 mm. The designed mask of FZP consists of 10 zones in which the inner ring of the FZP contains 200 pixels and 3 pixels as the outer ring (Figure 6A). Bright-field microscopy image of FZP (Figure 6B) shows a series of concentric annular rings, although the contrast between odd and even zones is difficult to distinguish due to the transparency of PEGDA. SEM image shows strong contrast between the annular grooves (black zones) and the crosslinked hydrogel rings (white zones) (Figure 6C).

The optical characteristics including light focusing and imaging performance of fabricated FZP were tested using He-Ne laser setup (Figure S1) and optical setup (Figure S2) respectively. The image of the focused beam can be seen in Figure 6D. The FZP produces a clear and well-defined focal spot with concentric diffractive rings whose full width at half maximum (FWHM) is around 18 μm (Figure 6E). An image of the capital letter “H” was used to analyze the imaging performance of FZP lens; Figure 6E shows a good quality image at the primary focusing length of 15.82 mm. To analyze optical properties at secondary focusing lengths, optical microscope set-up (Figure S2) was used; in this setup the light source was replaced with He-Ne laser to measure the focusing lengths (**red solid line in** Figure 6G). The experimental results match well with theoretical results (**black dashed line in** Figure 6G) calculated using Equation 6. Imaging performance under these focusing lengths were also characterized. As the focusing length decreased, the image size of “H” and corresponding diffraction efficiency decreases. (**Inset in** Figure 6G) The diffraction efficiency at the primary focus is around 35.7% which has the slight mismatch with the theoretical result 40.5% calculated by Equation 5, possibly attributed to absorption and scattering of the device. These results demonstrate that the fabricated FZP exhibits visible light focusing and imaging.

2.5 Fork-shaped grating

Diffractive optical elements such as spiral phase plate, helical axion, computer-generated holograms (CGH) as well as fork-shaped gratings can be used to generate the optical vortex beam. The transverse cross-sections of the optical vortices are associated with isolated point singularities with helical phase wavefront around them. The central singular point of the helix possesses undefined phase and therefore the intensity vanishing, leading to the

characteristic donut beam intensity profile.[48] In biomedical photonics, this special property if often used to manipulate biological cells and proteins.[49]

Here, we generate a binary CGH by simulating the interference of optical beams carrying a spiral phase and a tilted wave to obtain a fork grating (also called a vortex grating) which can be utilized to construct the optical vortex beam. The theoretical model of the simulation is presented in SI-3 (D). The vortex grating contains partially approximately parallel lines and has a bifurcated structure (a fork-like pattern) at the center of the pattern, as shown in Figure 7A. Phase contrast image shows the fork grating (white) and uncrosslinked prepolymer (black) in Figure 7C.

The optical characteristics of the fork grating in PEGDA was analyzed using He-Ne laser setup (Figure S1). The intensity pattern of the zero and first order diffraction is shown in Figure 7E, while the intensity distribution of the first diffraction order at the focus is shown in Figure 7F. The intensity is distributed in a donut shape, with the intensity of zero at the center (Figure 7G). The FWHM of the central gap is around 14.4 μm. The performance of the hydrogel-based fork grating to reconstruct the optical vortex beam demonstrates that it can be potentially applied for optical trapping and manipulation of single cell or particle in biophotonic integrated system.

2.6 Computer generated hologram (CGH) of arbitrary user-defined pattern

Digital masks of all optical components described in section 2 were CGHs generated from SCGH technique and then printed on PEGDA films, and subsequently reconstructed by coherent laser source to obtain the desired diffractive patterns. CGH is a kind of diffractive optical element that offers the possibility of creating display systems using digitally generating holographic interference patterns to reconstruct any arbitrary user-defined object.[40,50] To demonstrate the versatility of proposed digital photopatterning, we designed and fabricated the CGH of pattern ‘Syracuse University (SU) Logo’ shown in Figure 8A. Its digital mask was obtained by simulating the interference between Fourier pattern of SU logo and tilted plane wave (Figure 8B). The Fourier pattern of SU logo is generated by iterative Fourier transformation and optimization using Gerchberg-Saxton (GS) algorithm.[51] (Details are reported in SI-3E). The digital mask, which consists of an array of vertically microgrooves, was used as input pattern in digital projection photolithography and printed on hydrogel film. Figure 8C and Figure 8D are bright field image and phase contrast image of the printed device respectively. Figure 8E shows a close-up image of these microstructures with a feature resolution of 1 μm. The reconstruction of the CGH was characterized using the experimental set-up described in Figure S1. The fabricated device was mounted on a slide holder with a white screen located 100 mm away to capture the diffraction pattern. The white screen was aligned parallel to the surface place of the hologram substrate and a digital camera was placed in front of the screen. The coherent laser beam at 632.8 nm were normally positioned behind the hologram incident to the substrate. In the transmission mode, the first order diffraction pattern consisted of two symmetrical SU logo diffraction patterns located on the opposite sides of the center (zero order) (Figure 8F). The intensity of left and right sides in Figure 8F is slightly weak because of non-uniform illumination from He-Ne laser which follows a standard Gaussian intensity distribution.

These results indicate that CGH made in PEGDA can be potentially used to record and reconstruct any arbitrary pattern.

2.7 Robustness characterization of the printed hDOEs

To address concerns related to the robustness of the printed hDOEs, several control experiments were performed using Dammann Grating (DG) as a model hDOE. To assess the effects of water evaporation through PDMS, DG hDOEs were photo-patterned on PEGDA, and the 'as printed' samples (with sealed PDMS spacer) were left in air for 7 days. Brightfield images **(top row –** Fig. S10) show that the structure does not change during this period. Diffraction properties of the 'as printed' samples, tested using 632.8 nm He-Ne laser at normal incidence illumination, show that the changes in their optical (beam splitting) performance is not significant **(bottom row –** Fig. S10). To assess the effect of PDMS spacer removal, DG hDOEs were printed on Day 1, PDMS spacer was removed and the unreacted prepolymer was washed away, and samples were dehydrated in the desiccator for 1, 2, 3 and 4 hours **(top row:** Fig. S11). After the dehydration per each hour, samples were rehydrated in prepolymer solution **(middle row:** Fig. S11), and the diffraction properties were characterized. Results show that the changes in their optical (beam splitting) performance is not significant. **(bottom row:** Fig. S11). In another experiment, samples were printed on Day 1 and the optical performance of 'as printed' sample was obtained. Then, PDMS spacer was removed and the unreacted prepolymer was washed away, and samples were dehydrated in the desiccator for 4 hours before characterizing their optical performance. Then, sample was dehydrated for 7 more days in the desiccator and then the sample was rehydrated for few minutes and its optical performance was characterized. Results show that the changes in their optical (beam splitting) performance is not significant. These control experiments show that PEGDA 90% hDOE samples are robust, and the pattern fidelity and associated optical performance does not change during the dehydration and the rehydration processes.

To assess the effects of long-term laser exposure on printed hDOEs, samples were irradiated for several hours using the He-Ne laser (11mW), however no changes were recorded in the structure and the optical performance of hDOEs. To simulate long exposure durations, we repeated the same experiment with a femtosecond laser (wavelength: 800 nm, frequency: 80 MHz, pulse duration: 140 fs) with 1 W power. (Fig. S12) After more than 1 hour of exposure, pattern fidelity or the optical performance did not change. Only when a focused laser beam was used, the structure was ablated.

3. Discussion

Compact sizes of DOEs, widely used to gain control over light beam properties, are particularly attractive in miniaturization of complicated optical systems. In recent years, hydrogels have emerged as a promising material to develop hDOEs for a range of biomedical applications such as *in vivo* waveguides for light delivery, optical biosensors, optogenetic therapy, and optofluidic devices.[22] Unlike traditional materials which are stiff, difficult to process, and often non-biocompatible, hydrogel exhibits a unique hydrated network of cross-linked hydrophilic polymers making them optically transparent, inert,

flexible and biocompatible. However, hDOEs are not widely accepted in the field due to the challenges involved in design and fabrication of customized hDOEs for achieving target optical performance that is comparable to that of conventional materials. In this work, we demonstrate a new design and fabrication method to convert a widely used photosensitive hydrogel (PEGDA) into an array of optically functional hDOEs, which can be potentially used in the aforementioned applications.

Using PEGDA as our model hydrogel materials, we use digital photopatterning which integrates SCGH (for design of hDOEs) and digital projection photolithography (for fabrication of hDOEs) into a seamless and generic workflow for printing customized hDOEs. Based on user specifications/inputs, digital masks were generated using SCGH and patterned on PEGDA. The ability to customize and rapidly fabricate hDOEs was demonstrated by printing 1D/2D diffraction gratings, Dammann grating, Fresnel Zone Plate (FZP), fork-shaped grating and computer-generated hologram. As compared to conventional indirect methods such as molding, physical mask-based photolithography and dry etching, which are expensive and require exclusive access to microfabrication cleanroom facilities, digital photo-patterning is fast (~2sec per device) and customizable (no need to create a new master mold or a physical mask). As compared to conventional direct methods such as electron beam lithography, interference lithography and femtosecond laser micromachining, our method is inexpensive (no need for specialized and expensive instruments) and easy to implement (no need for technical expertise to operate the patterning platform effectively). As with other technologies, this patterning method also balances feature resolution and exposure overall size. To achieve high feature resolution (1 μm), the printing area in our setup was 2 mm ×1 mm. Although sub-micron feature resolution is possible by this technology with the use of higher magnification objectives such as 20× and 50×, this aspect has not been investigated in this report. In the future, this method can be scaled up by using high-resolution XY scanning and incorporating step-stitching printing strategy.

The optical performance of hDOEs, patterned in this work, was found to be comparable with DOEs made using conventional polymeric materials and fabrication methods as explained below. For instance, 1D/2D phase-type gratings show similar angular dispersion function as transmission grating fabricated (Figure 4E), while the transmission efficiency is over 70% which is higher than conventional amplitude type gratings which is less than 50%[26,52]. PEGDA Dammann grating shows 5×5 uniform beamlets at its Fourier plane (Figure 5). The intensity uniformity along X and Y direction is smaller than 20% comparable to previously reported Dammann grating made from resin.[53–55] PEGDA FZP (Section 2.4) has similar focusing and imaging function with reported FZP made from photoresist, protein and silk materials.[26,28,46] Experimental diffraction efficiency of PEGDA FZP is 35%; this is close to the theoretically calculated efficiency of 40% and higher than the one reported by amplitude-based FZP made in silk materials. PEGDA fork gratings presented a uniform optical vortex beam; devices with similar optical performance have been used for particle and cell manipulation.[49,56] Reconstruction of CGH in PEGDA can precisely record most of the optical information from the input in form of the ‘Syracuse University’ logo. The current design can be further improved by optimizing the algorithm used for SCGH. Although only 5 DOEs were presented in this work, any user-defined DOEs can be generated through SCGH and rapidly printed out using proposed high-resolution photolithography platform.

The potential use of hDOEs in the field is highlighted by the following examples. For instance, photonic microstructure printed on a glucose-selective hydrogel film changed its Bragg diffraction upon exposure to glucose. This film was combined with commercial contact lenses for point-of-care monitoring of glucose using smartphones. [23]In another study, DOEs made from silk hydrogel were developed to monitor both *in vitro* and *in vivo* drug release based on hydration-based diffraction.[25] In another study, soft diffractive micro-optics, called 'microscale kinoform phase-type lens' were generated by printing bovine serum albumin (BSA) protein on polydimethylsiloxane (PDMS) films. Laser shaping and imaging function were achieved using these flexible, stretchable, biocompatible and biodegradable lenses, with potential use in foldable optical devices. [28] Lastly, a recent review highlights the use of optically-functional devices such as waveguides, optical fibers, photonic crystals, and plasmonic structures by hydrogels doped with luminescent agents. [57] We envision that instead of replacing conventional photonic materials, hDOEs can be potentially used in applications that require a combination of optical performance and biocompatibility, biological inertness, and mechanical flexibility.

4. Conclusion

DOEs, which enable control over light via microstructural organization, have been widely used in imaging, diagnostics and biosensing. Recently, the demand for hydrogel based DOEs has surged as an alternative to conventional DOEs. To enable widespread use of hDOEs, key challenges related to customization and ease/speed of manufacturing need to be addressed. In this work, we report a new strategy to rapidly design and fabricate customized hDOEs using digital photopatterning technology. This facile approach enabled fast prototyping of hDOEs with optical performance comparable to optical devices made from conventional materials. This strategy can be potentially used to convert any photosensitive biomaterials into user-defined DOEs on demand, and help advance the use of hDOEs in integrative biophotonics and optofluidics applications in the future.

5. Experimental Section

PEGDA prepolymer preparation:

Poly (ethylene glycol) diacrylate (PEGDA, Mn=700) and PBS were purchased from Sigma-Aldrich and used without further modifications. The photointiator, LAP, was synthesized using previously established protocol. The prepolymer solution was composed of varying amounts of PEGDA (10% to 90%, v/v) with LAP (0.25%, w/v for all compositions). The prepolymer solution was mixed for 10 mins using a magnetic stirrer, filtered (pore size=0.2 μm), and used within 2 days after preparation. Before fabrication, 30 μL of the prepolymer solution was pipetted on a microscopic glass slide (48 mm × 24 mm, Fisher Scientific) that was surface modified using Sigmacote (Sigma-Aldrich). A PDMS spacer was placed between the microscope slide (bottom) and methacrylated glass coverslip (top) to control the prepolymer layer thickness to be 20 μm. (Figure 1 **inset)** The coverslip (top) was surface modified to ensure adhesion of crosslinked PEGDA layers during photo-patterning.

Synthesis of photoinitiator:

Lithium phenyl-2,4,6-trimethylbenzoylphosphinate (LAP) was synthesized in a two-step process according to established protocols[58]. At room temperature and under argon, 2,4,6-trimethyl-benzoyl chloride (4.5g, 25 mmol) was added dropwise to continuously stirred dimethyl phenylphosphonite (4.2g, 25 mmol). The reaction mixture was then stirred for 24 h and an excess of lithium bromide (2.4g, 28 mmol) into 50ml of 2-butanone was added to the reacted mixture which was then heated up to 50 °C. After 10 mins, a solid precipitate was observed. The mixture was cooled to room temperature, allowed to rest overnight and then filtered. The filtrate was washed with 2-butanone (3x with 25 ml) to remove unreacted lithium bromide and dried under vacuum to obtain LAP (6.2g, 22 mmol, 88%).

Methacrylation of glass coverslip:

Glass coverslips were immersed into 10% (w/v) NaOH solution for 30min, and washed in DI water, 75% (v/v) ethanol, and 100% ethanol (performed twice for 3min for each wash). The coverslip was subsequently dried using nitrogen. The dried coverslips then underwent methacrylation by immersing them for 12h in a solution comprised of 85mM 3-(Trimethoxysilyl) propyl methacrylate (TMSPM, Sigma) and ethanol solution with acetic acid (pH 4.5). Finally, the coverslips were washed with ethanol three times and baked for 1h at 100°C.

Optical and mechanical characterization of PEGDA:

Refractive indices of prepolymer and crosslinked samples were measured with digital refractometer (Sper Scientific). To measure optical transparency, prepolymer were prepared in standard 1 cm-wide disposable cuvettes, and optical attenuation was measured using scanning spectrophotometer from 250 to 1100 nm (Thermo Scientific). Mechanical properties were measured using a standard Rheometer (AR2000, TA Instruments, USA). Briefly, samples were prepared by casting the prepolymer solution in PDMS mold (8 mm diameter, 100 μm thickness) and exposing samples to UV light (output power 70 mw cm^{-2}, Ominicure S2000) for 2 minutes. The crosslinked samples were then transferred to the well plates and incubated in ultra-pure DI water for 24 hours to facilitate diffusion of uncrosslinked prepolymer. Next, samples were tested at 25 °C using 8 mm diameter bottom plate with a gap of 0.5 mm. Storage modulus (G') and loss modulus (G") were measured at 0.5% strain for a range of 0.1–100 Hz. Elastic modulus was calculated by the following Equation 3 where the Poisson ratio τ was assumed as 0.33. The linear regions of both moduli recorded between 1 and 10 Hz were used to calculate the Elastic modulus (E).[59]

$$E = 2G(1+\tau) \text{Where} G = \sqrt{G'^2 + G''^2} \quad (3)$$

Digital projection photolithography setup:

The setup consists of three main components: the DLP development kit (DLP 1080p 9500 UV, Texas Instruments, USA), a UV lamp (Ominicure S2000, Canada) and an UV 10× projection lens (Thorlabs, USA) (Figure 1). Light irradiated from UV lamp was filtered to obtain a central wavelength 405 nm, and further homogenized, collimated and expanded by

illumination optics before directing onto the Digital Micromirror Device (DMD). The DMD used in this system consists of 1920 × 1080 array of micromirrors with single pixel resolution of 10.8 μm. To fabricate customizable diffractive micro-optics, digital masks were designed and uploaded onto the DMD. The DMD generates virtual masks which dynamically modulates the irradiated UV light into customized light patterns. A projection lens was used to de-magnify the light patterns and project them onto PEGDA prepolymer between the bottom glass slide and top coverslip, which facilitate selective crosslinking of exposed areas. All micro-optics elements reported in this study required an exposure time of 2 seconds and an UV light intensity of 70 mW cm^{-2}.

Design of DOEs using simulated computer-generated holography:

Customized MATLAB algorithms based on computer generated holography were written to generate digital masks for printing customized diffractive micro-optical devices in PEGDA. The generic process flow includes 4 steps (Figure 2): (1) User design type/specifications, (2) simulated computer-generated holography (SCGH), (3) interference pattern generation and (4) digital mask for DMD. For instance, in step 1, the user can specify design type as ‘diffraction’ (1D or 2D) and the spacing of grating as inputs. In step 2, the input parameters will be used as initial conditions for the SCGH codes in MATLAB. In this case, the SCGH of diffraction grating is the interference between two plane waves, where the angle between two beams determine the groove spacing. In step 3, the set angle is used to generate the interference pattern with defined groove spacing. Finally, in step 4, the interference pattern will be binarized to generate a digital mask for the DMD. This generic process was followed to design and print 1D and 2D diffraction gratings, Dammann grating, Fresnel zone plate, fork-shaped grating and computer-generated hologram of arbitrary pattern in model PEGDA hydrogel. This strategy allows the generation of micro-optical elements with predefined or customized optical properties. For each diffractive micro-optical element, details of masks are presented in Section 2 while theoretical models to generate corresponding SCGH are described in section SI-3.

Characterization of printed devices:

(1) Characterization of micro-patterns. Printed micro-patterns for all devices were characterized using optical microscope, phase-contrast microscope and scanning electron microscope (SEM). The samples for optical microscope (Observer X1, Zeiss, Germany) and phase-contrast microscope (Lecia DM6000, Germany) were kept hydrated. For obtaining SEM images, printed PEGDA samples were separated from their PDMS spacer, washed 3 times with PBS to wash out the unreacted prepolymer, before lyophilizing in a freeze dryer (Labconco, Kansas City, MO) for 24hours. Then the samples were sputter coated with a layer of gold (35 seconds) and imaged under SEM with 8kV eV. (JEOL5600, Japan).

(2) Characterization of optical properties. The details of the setup used to characterize the optical properties of printed devices is illustrated in Figures S1 and S2. The setup in Figure S1 is used to characterize the diffraction pattern and diffraction efficiency while the setup in Figure S2 is used to characterize the imaging performance of FZP. Equations 4, 5 and 6 were used to characterize the optical properties of selected DOEs as described below:

Dammann grating: Intensity uniformity of array beams output from Dammann grating[47]

$$U = \frac{I_{max} - I_{min}}{I_{max} + I_{min}} \quad (4)$$

Where U is defined as intensity uniformity, I_{max} is the maximum grayscale intensity of single spot and I_{min} is the minimum grayscale intensity of single spot.

Fresnel Zone Plate (FZP): Diffraction efficiency of FZP is given by[46,60]

$$\eta(n) = \frac{sin^2\left(\frac{\pi}{n}\right)}{\frac{\pi}{n}} = sinc^2(1/n) \quad (5)$$

Where η is defined as diffraction efficiency of phase type FZP and n is the level of zone rings which is 2 in this work.

Focusing length of phase type FZP

$$f = \frac{r_N{}^2}{N\lambda} \quad (6)$$

Where r_N is the radius of successive zones (here is the radius of first ring), f is the focusing length, λ is the wavelength and N is positive integer which is from 1 to 10 in this work.

Supplementary Material

Refer to Web version on PubMed Central for supplementary material.

Acknowledgements

This work was partially supported by NIH R21GM129607 and R21AR076645 awarded to Prof. Pranav Soman.

References

[1]. Zhang YS, Khademhosseini A, Science (80-.) 2017, 356, DOI: 10.1126/science.aaf3627.
[2]. Elisseeff J, Nat. Mater 2008, 7, 271. [PubMed: 18354410]
[3]. Kopeček J, Biomaterials 2007, 28, 5185. [PubMed: 17697712]
[4]. El-Sherbiny IM, Yacoub MH, Glob. Cardiol. Sci. Pract 2013, 2013, 38.
[5]. Kunwar P, Xiong Z, Zhu Y, Li H, Filip A, Soman P, Adv. Opt. Mater 2019, 7, 1900656.
[6]. Xiong Z, Li H, Kunwar P, Zhu Y, Ramos R, McLoughlin S, Winston T, Ma Z, Soman P, Biofabrication 2019, 11, 35005.
[7]. Sanchez-Dealcazar D, Romera D, Castro-Smirnov J, Sousaraei A, Casado S, Espasa A, Morant-Miñana MC, Hernandez JJ, Rodríguez I, Costa RD, Cabanillas-Gonzalez J, Martinez RV, Cortajarena AL, Nanoscale Adv. 2019, 1, 3980.
[8]. Huang T, Xu H, Jiao K, Zhu L, Brown HR, Wang H, Adv. Mater 2007, 19, 1622.
[9]. Lawrence BD, Cronin-Golomb M, Georgakoudi I, Kaplan DL, Omenetto FG, Biomacromolecules 2008, 9, 1214. [PubMed: 18370418]
[10]. Kotwal A, Schmidt CE, Biomaterials 2001, 22, 1055. [PubMed: 11352099]
[11]. Hoare TR, Kohane DS, Polymer (Guildf). 2008, 49, 1993.

[12]. Zhang Y, Yang B, Zhang X, Xu L, Tao L, Li S, Wei Y, Chem. Commun 2012, 48, 9305.
[13]. Zhou K, Bisoyi HK, Jin J, Yuan C, Liu Z, Shen D, Lu Y, Zheng Z, Zhang W, Li Q, Adv. Mater 2018, 30, 1800237.
[14]. Zheng Z, Yuan C, Hu W, Bisoyi HK, Tang M, Liu Z, Sun P, Yang W, Wang X, Shen D, Adv. Mater 2017, 29, 1703165.
[15]. Poleshchuk AG, Churin EG, Koronkevich VP, Korolkov VP, Kharissov AA, Cherkashin VV, Kiryanov VP, Kiryanov AV, Kokarev SA, Verhoglyad AG, Appl. Opt 1999, 38, 1295. [PubMed: 18305745]
[16]. Swanson GJ, Binary Optics Technology : The Theory and Design of Multi-Level Diffractive Optical Elements, MASSACHUSETTS INST OF TECH LEXINGTON LINCOLN LAB, 1989.
[17]. Gale MT, Microelectron. Eng 1997, 34, 321.
[18]. Gale MT, Rossi M, Schütz H, Ehbets P, Herzig HP, Prongué D, Appl. Opt 1993, 32, 2526. [PubMed: 20820413]
[19]. Shan D, Gerhard E, Zhang C, Tierney JW, Xie D, Liu Z, Yang J, Bioact. Mater 2018, 3, 434. [PubMed: 30151431]
[20]. Vörös J, Ramsden JJ, Csúcs G, Szendro I, De Paul SM, Textor M, Spencer ND, Biomaterials 2002, 23, 3699. [PubMed: 12109695]
[21]. Chao W, Kim J, Rekawa S, Fischer P, Anderson EH, Opt. Express 2009, 17, 17669. [PubMed: 19907552]
[22]. Xiong R, Luan J, Kang S, Ye C, Singamaneni S, Tsukruk VV, Chem. Soc. Rev 2020, 49, 983. [PubMed: 31960001]
[23]. Elsherif M, Hassan MU, Yetisen AK, Butt H, ACS Nano 2018, 12, 2283. [PubMed: 29529366]
[24]. Yetisen AK, Naydenova I, da Cruz Vasconcellos F, Blyth J, Lowe CR, Chem. Rev 2014, 114, 10654. [PubMed: 25211200]
[25]. Zhou Z, Shi Z, Cai X, Zhang S, Corder SG, Li X, Zhang Y, Zhang G, Chen L, Liu M, Kaplan DL, Omenetto FG, Mao Y, Tao Z, Tao TH, Adv. Mater 2017, 29, 1.
[26]. Pal RK, Kurland NE, Wang C, Kundu SC, Yadavalli VK, ACS Appl. Mater. Interfaces 2015, 7, 8809. [PubMed: 25853731]
[27]. Yin MJ, Yao M, Gao S, Zhang AP, Tam HY, Wai PKA, Adv. Mater 2016, 28, 1394. [PubMed: 26643765]
[28]. Sun YL, Dong WF, Niu LG, Jiang T, Liu DX, Zhang L, Wang YS, Chen QD, Kim DP, Sun HB, Light Sci. Appl 2014, 3, e129.
[29]. Kurland NE, Dey T, Kundu SC, Yadavalli VK, Adv. Mater 2013, 25, 6207. [PubMed: 24038619]
[30]. Nie Z, Kumacheva E, Nat. Mater 2008, 7, 277. [PubMed: 18354414]
[31]. Humar M, Kwok SJJ, Choi M, Yetisen AK, Cho S, Yun SH, Nanophotonics 2017, 6, 414.
[32]. Sun C, Fang N, Wu DM, Zhang X, Sensors Actuators A Phys. 2005, 121, 113.
[33]. Xiong Z, Liu H, Chen R, Xu J, Li Q, Li J, Zhang W, Opt. Express 2018, 26, 18597. [PubMed: 30114036]
[34]. Xiong Z, Liu H, Tan X, Lu Z, Li C, Song L, Wang Z, J. Micro/Nanolithography, MEMS, MOEMS 2014, 13, 043016.
[35]. Zhang Y, Luo J, Xiong Z, Liu H, Wang L, Gu Y, Lu Z, Li J, Huang J, Opt. Express 2019, 27, 31956. [PubMed: 31684417]
[36]. Grigoryan B, Paulsen SJ, Corbett DC, Sazer DW, Fortin CL, Zaita AJ, Greenfield PT, Calafat NJ, Gounley JP, Ta AH, Johansson F, Randles A, Rosenkrantz JE, Louis-Rosenberg JD, Galie PA, Stevens KR, Miller JS, Science (80-.) 2019, 364, 458.
[37]. Tumbleston JR, Shirvanyants D, Ermoshkin N, Janusziewicz R, Johnson AR, Kelly D, Chen K, Pinschmidt R, Rolland JP, Ermoshkin A, Samulski ET, DeSimone JM, Science (80-.) 2015, 347, 1349.
[38]. Zheng X, Lee H, Weisgraber TH, Shusteff M, DeOtte J, Duoss EB, Kuntz JD, Biener MM, Ge Q, Jackson JA, Kucheyev SO, Fang NX, Spadaccini CM, Science (80-.) 2014, 344, 1373.
[39]. Kunwar P, Jannini AVS, Xiong Z, Ransbottom MJ, Perkins JS, Henderson JH, Hasenwinkel JM, Soman P, ACS Appl. Mater. Interfaces 2020, 12, 1640. [PubMed: 31833757]

[40]. Lee W-H, Appl. Opt 1979, 18, 3661. [PubMed: 20216666]
[41]. Leith EN, Introduction to Fourier Optics, Roberts And Company Publishers, 1969.
[42]. Wyrowski F, J. Opt. Soc. Am. A 1990, 7, 961.
[43]. Wu YH, Park HB, Kai T, Freeman BD, Kalika DS, J. Memb. Sci 2010, 347, 197.
[44]. Choi M, Choi JW, Kim S, Nizamoglu S, Hahn SK, Yun SH, Nat. Photonics 2013, 7, 987. [PubMed: 25346777]
[45]. Bolin FP, Preuss LE, Taylor RC, Ference RJ, Appl. Opt 1989, 28, 2297. [PubMed: 20555515]
[46]. Chen QD, Wu D, Niu LG, Wang J, Lin XF, Xia H, Sun HB, Appl. Phys. Lett 2007, 91, 171105.
[47]. Krackhardt U, Streibl N, Opt. Commun 1989, 74, 31.
[48]. Cai X, Wang J, Strain MJ, Johnson-Morris B, Zhu J, Sorel M, O'Brien JL, Thompson MG, Yu S, Science (80-.) 2012, 338, 363.
[49]. Jeffries GDM, Edgar JS, Yiqiong Z, Shelby JP, Christine F, Chiu DT, Nano Lett. 2007, 7, 415. [PubMed: 17298009]
[50]. Slinger C, Cameron C, Stanley M, Computer (Long. Beach. Calif) 2005, 38, 46.
[51]. Zalevsky Z, Dorsch RG, Mendlovic D, Opt. Lett 1996, 21, 842. [PubMed: 19876177]
[52]. Alqurashi T, Montelongo Y, Penchev P, Yetisen AK, Dimov S, Butt H, Nanoscale 2017, 9, 13808. [PubMed: 28891581]
[53]. Wang W, Zhou C, Jia W, Appl. Opt 2008, 47, 1427. [PubMed: 18382567]
[54]. Chen Q-D, Lin X-F, Niu L-G, Wu D, Wang W-Q, Sun H-B, Opt. Lett 2008, 33, 2559. [PubMed: 18978920]
[55]. Li Y, Watanabe W, Tamaki T, Nishii J, Itoh K, Japanese J Appl. Physics, Part 1 Regul. Pap. Short Notes Rev. Pap 2005, 44, 5014.
[56]. Gahagan KT, Swartzlander GA, Conf. Proc. - Lasers Electro-Optics Soc. Annu. Meet 1996, 21, 155.
[57]. Umar M, Min K, Kim S, APL Photonics 2019, 4, 120901.
[58]. Fairbanks BD, Schwartz MP, Bowman CN, Anseth KS, Biomaterials 2009, 30, 6702. [PubMed: 19783300]
[59]. Qin XH, Wang X, Rottmar M, Nelson BJ, Maniura-Weber K, Adv. Mater 2018, 30, 1705564.
[60]. Buralli DA, Morris GM, Rogers JR, Appl. Opt 1989, 28, 976. [PubMed: 20548597]

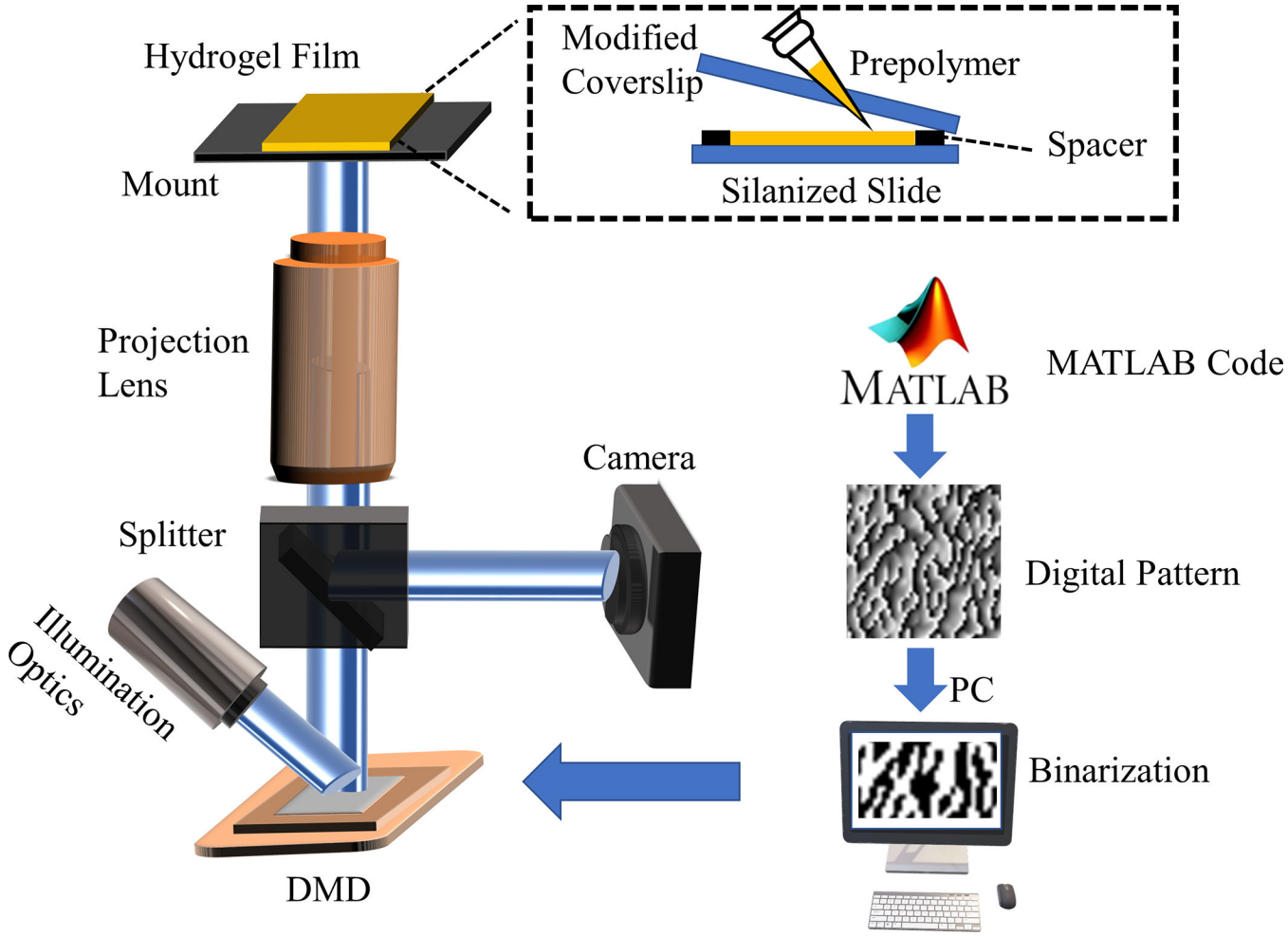

Figure 1.

Schematic of digital projection photolithography setup that consists of illumination optics, DMD, beam splitter, projection lens, CMOS camera and sample mount. The digital mask for customized diffractive optics, generated using MATLAB algorithm (Section 5), was fed to the DMD to generate virtual digital mask for UV light modulation via the DMD. Inset shows the setup for hydrogel film; Prepolymer solution is sandwiched between methacrylated coverslip and silanized microscope slide with PDMS spacer for thickness control.

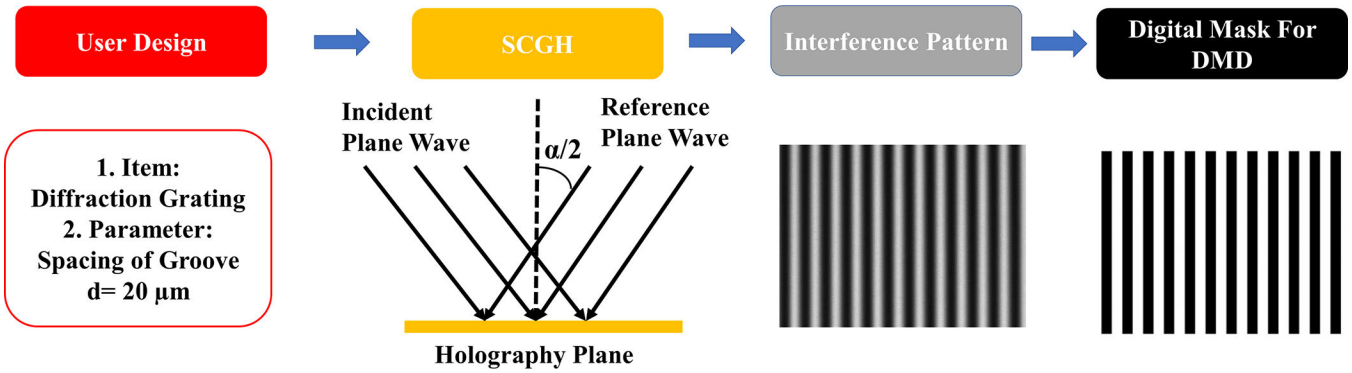

Figure 2.

Generic process flow to generate customized digital mask based on defined inputs. Here, 1D diffraction grating is chosen as a case study.

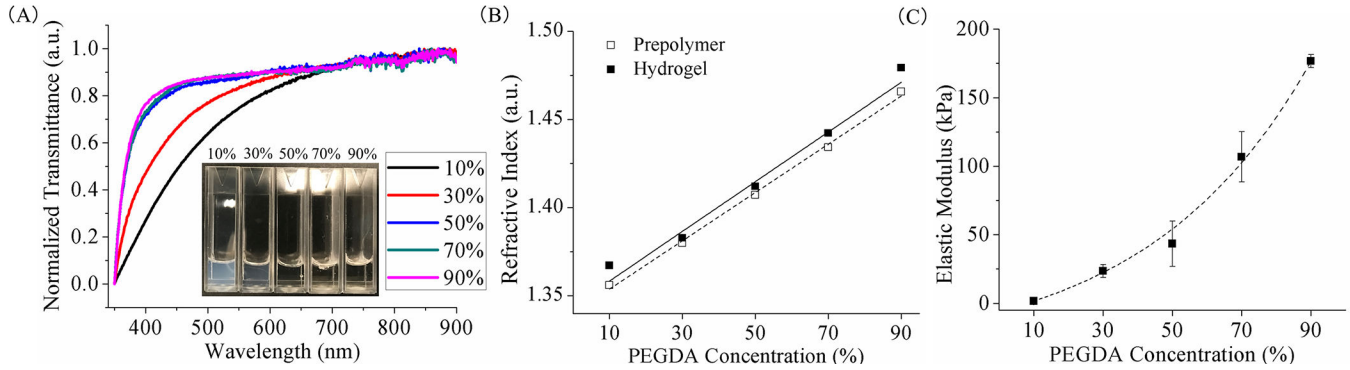

Figure 3.

Optical and mechanical characteristics of PEGDA hydrogels with varying prepolymer concentrations. (A) Optical transmission spectrum of PEGDA hydrogels. Inset shows photographs of PEGDA hydrogels in cuvette. (B) Refractive indices (RI) of crosslinked (solid) and uncrosslinked (dashed) PEGDA. (C) Elastic modulus of crosslinked PEGDA samples.

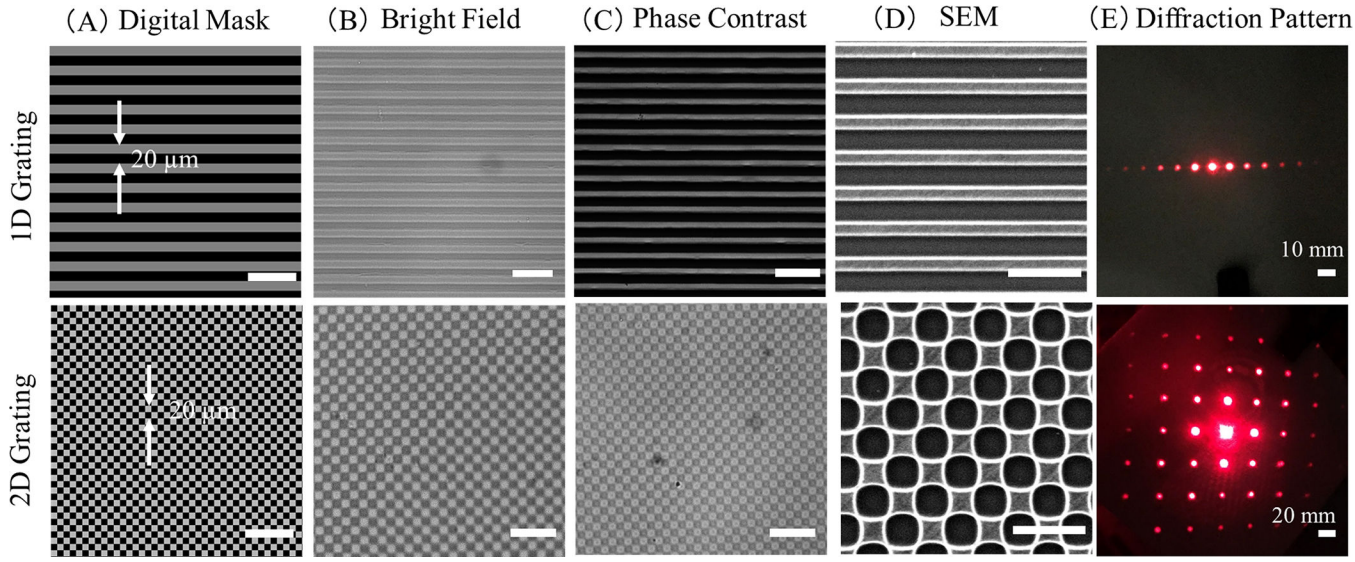

Figure 4.

Photo-patterning of 1D and 2D diffraction/transmission grating and characterization of their optical properties. (A) Designed patterns. The fabricated grating microstructures were characterized using bright-field microscopy (B), phase contrast microscopy (C) and SEM (D). (E) 2D views of grating diffraction pattern using 632.8 nm He-Ne laser at normal incidence illumination. Scale bar for A-D: 50 μm.

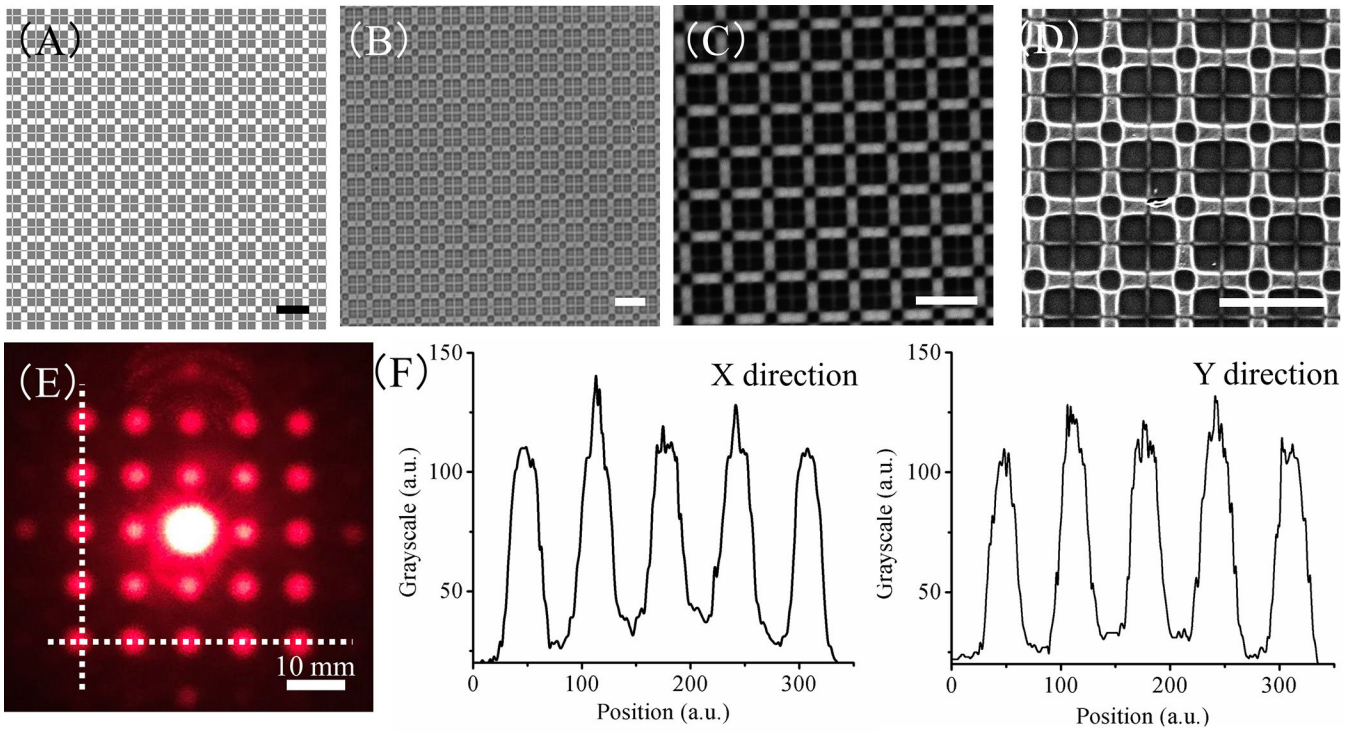

Figure 5.

Photo-patterning of PEGDA DG device and its optical characterization. (A) Designed mask pattern of 5 ×5 DG. The fabricated structure was characterized using bright-field microscopy (B) and phase contrast microscopy (C). (D) SEM image shows the close-up view of the micro-structure. (E) Beam splitting performance and intensity cross-section (dotted lines in E) of individual beams along X and Y axis (F). Scale bar A-D: 20 μm.

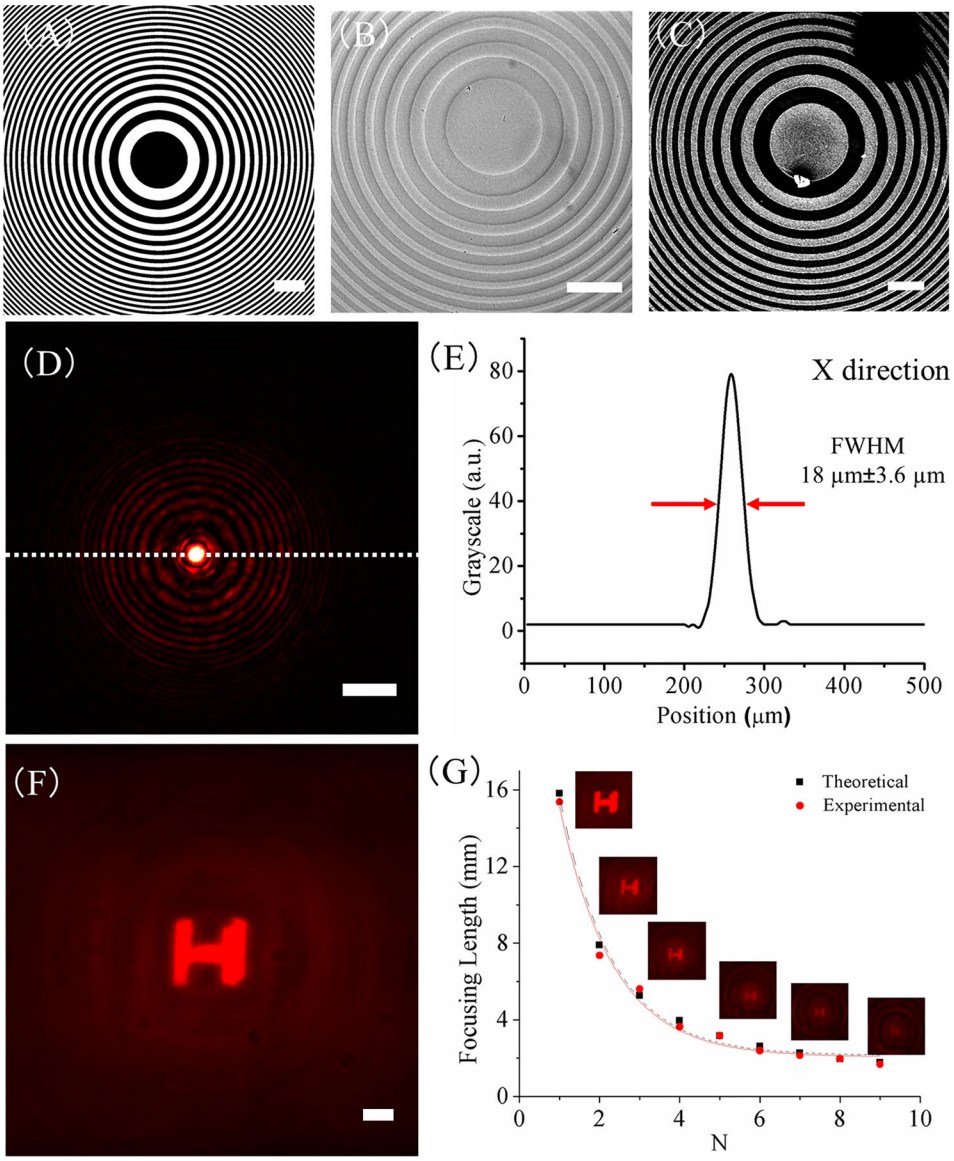

Figure 6.

Photo-patterning of FZP in PEGDA and characterization of its optical properties. (A) Designed digital mask of FZP. Images of FZP fabricated from PEGDA were obtained using bright-field microscopy (B) and SEM (C). (D) Image of light focusing by FZP using He-Ne laser. (E) Intensity cross section of focal spot along X direction (dashed line in D). (F) Imaging performance of FZP using a capital letter ‘H’. (G) Theoretical and experimental results of primary and secondary focusing lengths. Inset shows the imaging performance for different focus lengths. Scale bar: 100 μm.

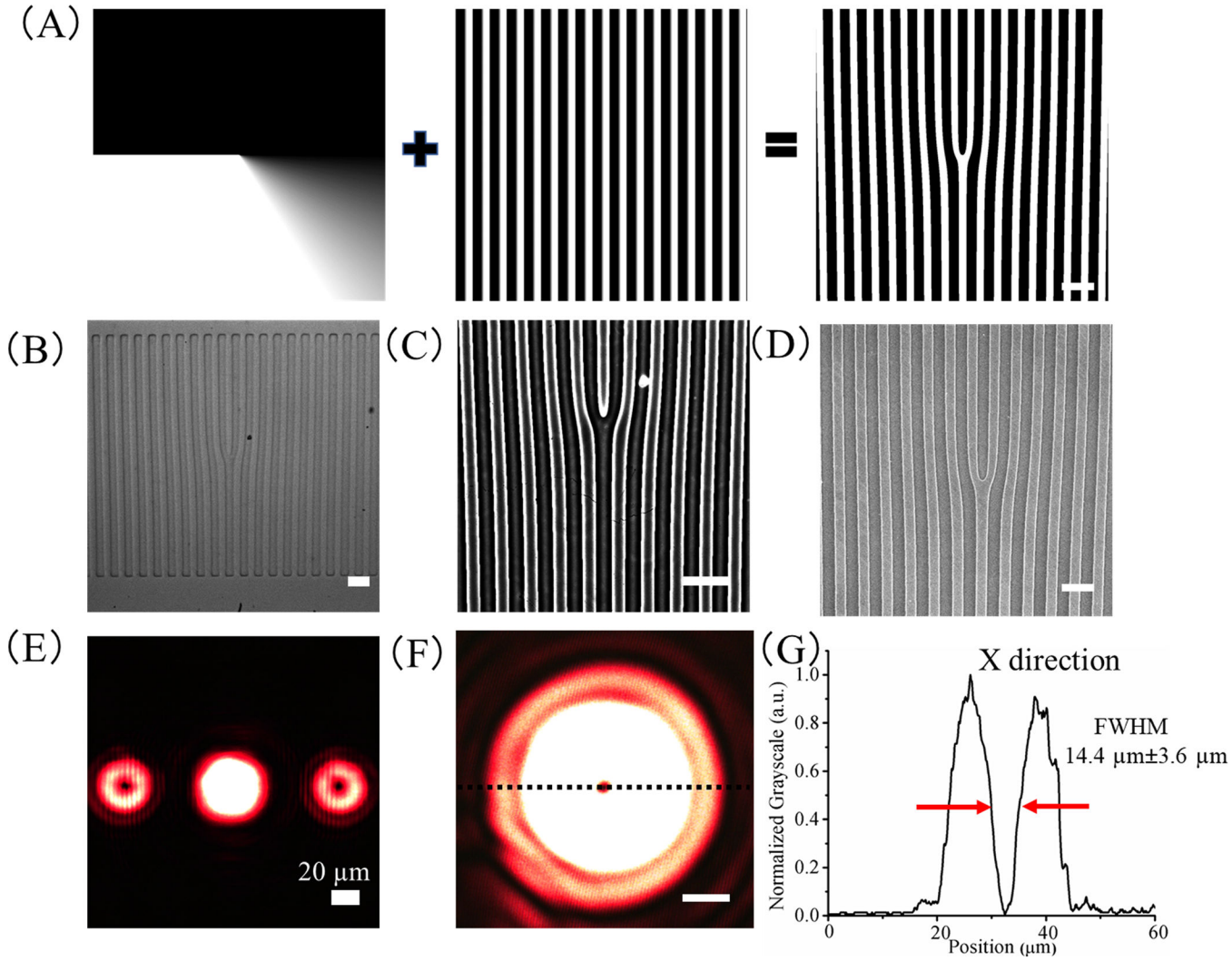

Figure 7.

Photo-patterning of fork grating and characterization of its optical properties. (A) Generation of digital mask of fork grating by simulating the interference between the optical beams carrying vortex phase and a tilted plane wave. The fabricated fork grating was characterized using bright-field (B) and phase contrast microscopy (C). (D) SEM image. (E) Optical characterization of diffraction pattern (0^{th} and 1^{st} diffraction orders) of fork grating using He-Ne laser. (F) Donut beam of fork grating at the focus and (G) its cross-section of intensity profile in X direction. Scale bar A-D and F: 100μm.

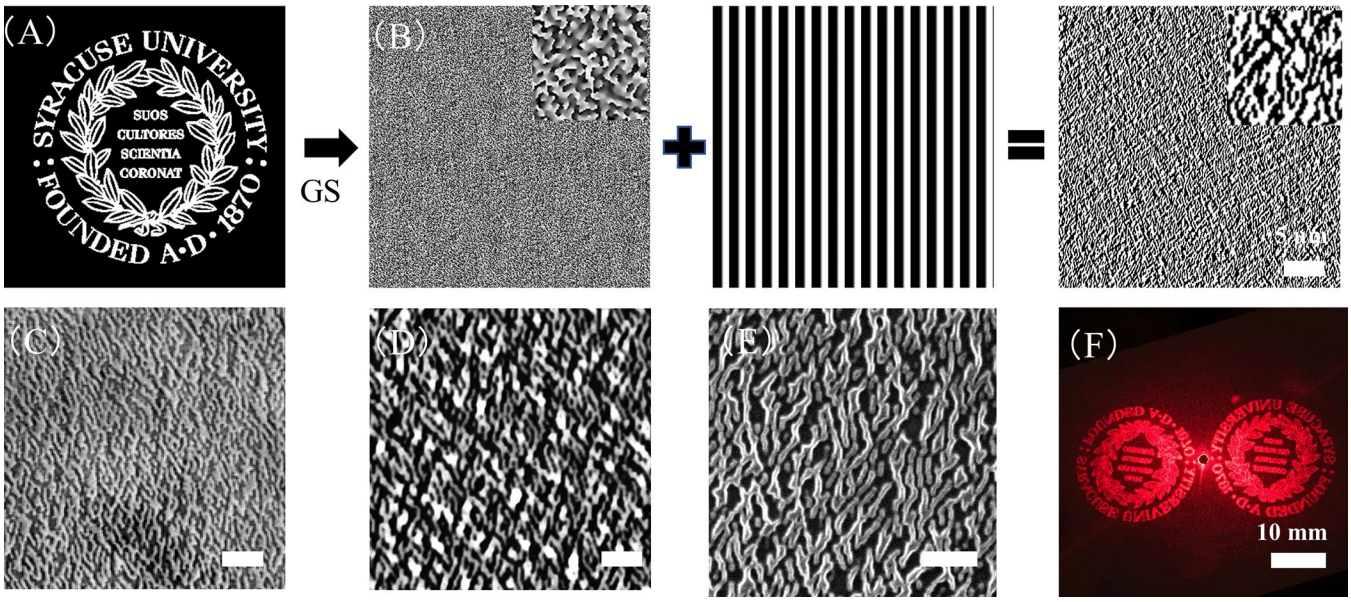

Figure 8.

Photo-patterning of CGH in PEGDA and characterization of its optical properties. (A) Desired reconstructed pattern of ‘Syracuse University (SU) Logo’. (B) Generation of digital mask of CGH using the GS algorithm. The CGH of SU logo is interfered with the tilted plane wave to obtain the digital mask for DMD. The fabricated CGH samples were characterized using bright field (C), phase contrast microscopy (D), and SEM (E). (F) The reconstructed diffraction pattern of CGH using He-Ne laser. Scale bar C-E: 20 μm.